Dynamics of sustained reentry in a loop model with discrete gap junction resistances

Wei Chen,* Mark Potse,† and Alain Vinet‡

Department of Physiology, Institute of Biomedical Engineering, Université de Montréal, Montréal, Canada H4J-1C5 and Centre de Recherche de l'Hôpital du Sacré-Coeur de Montréal, Montréal, Canada H4J-1C5

(Received 29 March 2007; revised manuscript received 25 July 2007; published 31 August 2007)

The dynamics of reentry is studied in a one-dimensional loop of model cardiac cells with discrete intercellular gap junction resistance (R). Each cell is represented by a continuous cable with ionic current given by a modified Beeler-Reuter formulation. For R below a limiting value, propagation is found to change from period-1 to quasiperiodic (QP) at a critical loop length (L_{crit}) that decreases with R. Quasiperiodic reentry exists from L_{crit} to a minimum length ($L_{\min}$), which also shortens with R. The decrease of $L_{crit}(R)$ is not a simple scaling, but the bifurcation can still be predicted from the slope of the restitution curve giving the duration of the action potential as a function of the diastolic interval. However, the shape of the restitution curve changes with R. An increase of R does not seem to increase the number of possible QP solutions since, as in the continuous cable, only two QP modes of propagation were found despite an extensive search through alternative initial conditions.

DOI: 10.1103/PhysRevE.76.021928 PACS number(s): 87.19.Hh, 05.45.−a

I. INTRODUCTION

Self-sustained propagation of electrical activity around a one-dimensional (1D) loop of cardiac tissue is the simplest model of reentry, the mechanism by which a propagating activation front maintains itself by traveling around a functional or anatomical obstacle. Reentry has been much studied because it was demonstrated to be an important mechanism of cardiac arrhythmia [1–4]. For the 1D loop, most work has been done assuming the membrane to be a continuous and uniform cable with constant intracellular axial resistivity [5–15]. For different models representing the ionic properties of the membrane, propagation was found to change from stable period-1 propagation to quasiperiodic reentry when the length of the loop was reduced below a critical length. The quasiperiodic reentry was characterized by a spatial oscillation of the action potential duration as propagation proceeded around the loop. Based on numerical simulations, the bifurcation was in most cases classified as supercritical, with the amplitude of the oscillation growing as the length of the loop was reduced below the critical length. Quasiperiodic reentry was found to exist from the critical length to a minimal length below which sustained propagation became impossible. In some instances, two different modes of quasiperiodic propagations were identified, with different wavelengths, different intervals of existence, and sometimes different scenarios of creation [6–10]. Various attempts were made to build simplified representations of the dynamics allowing analytical examination of the nature of the bifurcation [7,10,11,16–18]. One of these approaches, which guides the present investigation, relies on an integral-delay model [9,10]. It is based on the assumption that both the speed of propagation and the action potential duration can be expressed as functions of the diastolic interval, which measures the recovery time from the end of the previous action potential. The model has been successful in reproducing the locus of the bifurcation observed by numerical simulations of 1D loops with Beeler-Reuter-type representations of the membrane. It predicts that the bifurcation should occur when the diastolic interval in the period-1 reentry reaches the critical value where the slope of the restitution curve becomes 1.

However, cardiac excitable tissue is not a syncytium, but rather a mesh of myocytes connected by discrete gap junction resistances [19]. Much work has been done to investigate the effect of discrete resistances in a one-dimensional structure [14,20–24], many focused on the effect of resistivity on excitability. In the discrete case, the resistance no longer acts as a scaling factor with regard to space. Because the intercellular current is reduced as the gap junction resistance is increased, the latency of the cell-to-cell propagation is augmented until propagation fails at some limiting value of the resistance. Besides, upon premature or repetitive stimulations, the excitability of the tissue must be more recovered for propagation to proceed, which corresponds to an increase of the refractory period. Discrete coupling has also been to shown to act on the dynamics of propagation during reentry and pacing by modifying the repolarization, thereby changing the duration of the action potentials [25–27].

This paper describes how the bifurcation from period-1 to quasiperiodic propagation and the characteristics of the quasiperiodic (QP) propagation are modified by the increase of the intercellular resistance in a 1D loop of discrete model cardiac cells. This paper is organized as follows. In Sec. II, the model and computational method are described. The results of the numerical simulation are presented in Sec. III. The bifurcation from stable period-1 reentry is explained in Sec. IV. The QP modes of reentry are analyzed in Sec. V. The final section is devoted to a summary and discussion.

II. METHODS

We consider a one-dimensional loop formed by N identical cells connected by gap junction resistances. Each cell is

*wei.chen@umontreal.ca
†mark@potse.nl
‡alain.vinet@umontreal.ca

modeled as a continuous and uniform cable of radius (a) 5 μm, length (L_c) 100 μm, and intracellular resistivity (ρ) 0.2 kΩ cm lying in an unbounded volume conductor of negligible resistivity. The transmembrane potential ($V^{i=1,N}$ in mV) of the cells is described by the well-known cable equation

$$\frac{1}{\rho}\frac{\partial^2 V^i(x,t)}{\partial x^2} = S\left[C_m\frac{\partial V^i(x,t)}{\partial t} + I^i_{ion}(x,t)\right],$$

$$x \in \{0, L_c\}, \quad i \in \{1, N\}, \tag{1}$$

in which C_m is the membrane capacitance (1 μF/cm^2), S is the surface-to-volume ratio (0.4 μm^{-1}), and I_{ion} is the ionic current (μF/cm^2). The membrane ionic model is the same modified Beeler-Reuter (MBR) model that was used in our previous works on continuous 1D and 2D rings [6–8,28,29]. In this model, the sodium current is controlled by an activation gate variable m and two inactivation gate variables h and j. The plateau and repolarization of the action potential involve a gate-controlled calcium current as well as a gate-controlled and a voltage-dependent potassium current. Each cell is connected to its neighbors by a discrete gap junction resistance R (kΩ). Continuity of the intracellular current between the cells yields the boundary conditions [20]

$$\left.\frac{\partial V^i}{\partial x}\right|_{x=L_c} = \left.\frac{\partial V^{\mathrm{mod}(i,N)+1}}{\partial x}\right|_{x=0} = -\frac{\rho}{\pi a^2} I_{i,\mathrm{mod}(i,N)+1},$$

$$V^i(L_c) - V^{\mathrm{mod}(i,N)+1}(0) = R I_{i,\mathrm{mod}(i,N)+1}. \tag{2}$$

For simulation, we have modified the numerical method that we developed for continuous loops [6]. Briefly, for each time step (Δt=2 μs), Eq. (1) becomes equivalent to an ordinary differential equation

$$\frac{d^2 V^i(x)}{dx^2} - K^2 V^i(x) = g^i(x), \tag{3}$$

whose solution can be expressed as the sum of a particular solution $V^i_p(x)$ and of the homogeneous solution

$$V^i_h(x) = A_i e^{kx} + B_i e^{-kx}. \tag{4}$$

$V^i_p(x)$ is obtained by solving Eq. (3) with Neumann boundary conditions ($\partial V^i/\partial x|_{x=0,L_c}=0$) using a Galerkin finite-element method projected onto a linear basis function [13] with a uniform grid (Δx=25 μm)—i.e., five nodes. Cells are then reconnected by choosing the coefficients of the homogeneous solutions to fulfill the continuity conditions given by Eq. (2). For a subset of R values, calculations repeated with Δx=12.5 μm and Δt=1 μs gave the same results.

The purpose of the simulations is to obtain a description of the regimes of reentry of the function R and $L=NL_c$, the length of the loop. During reentry, the successive action potentials ($s=1,l$) at each node can be characterized by their activation times (T^s_{act}), set at the maximum derivative of the upstroke, and their repolarization times (T^s_{repol}), taken at the −50-mV down-crossing in repolarization. The action potential duration (A) and the diastolic interval (D) associated with each action potential are calculated, respectively, as $A^s = T^s_{repol} - T^s_{act}$ and $D^s = T^s_{act} - T^{s-1}_{repol}$ [5–8]. The propagation of the wave front along the loop generates spatial profiles of A and D that typify the reentry. In contrast to a continuous loop, propagation on a discrete loop can be patterned inside each cell, but identical across all the cells. We have chosen to use only A and D values of the middle node of all cells to characterize the reentries. We label period-1 ($P1$) reentries in which A and D remain constant across all the middle nodes and QP reentries where A and D oscillate both in time and space. The label "quasiperiodic" was used by analogy with the results of the analysis of integral-delay model done by Courtemanche *et al.* [9,10], but no further processing was done to clarify the exact nature of these nonconstant solutions.

For each value of R, an initial L was chosen large enough to sustain $P1$ stable reentry. Reentry was initiated by transiently opening the loop and stimulating one end. Computation was continued until stable period-1 reentry was detected, the stability criteria being less than 0.5 ms difference in A and D between all middle nodes for one rotation of the front. Afterward, the loop length was gradually reduced by steps of one cell, using the final state of the previous L as initial condition and removing one cell far from the position of the excitation front. When the stability criterion was not fulfilled after a minimum of 25 turns, reentry was labeled as QP. With this procedure, both L_{crit} and P_{crit}—respectively, the minimum length and minimum period with $P1$ reentry—as well as $L_{\min}$—the minimum length for sustained reentry—were identified for each value of R. In some instances, bistability between $P1$ and QP reentry was investigated by stepwise expanding loops that were initially in the quasiperiodic regime. One cell was inserted in the loop, with initial conditions set at the mean of the states of its neighboring cells. Finally, we also searched for distinct modes of QP reentry using the method described in [7], in which the D spatial profile of a QP solution for a given L value is compressed by a scaling factor to construct initial conditions to find alternative QP solutions with smaller wavelengths.

III. RESULTS

Figure 1(a) shows L_{crit} and $L_{\min}$ as a function of R. Both L_{crit} and $L_{\min}$ decrease until they merge at $R \simeq 104$ kΩ. From this resistance, QP reentry does not exist anymore and $P1$ reentry remains the only regime of sustained propagation. From there, the limiting length for $P1$ reentry increases until sustained propagation becomes impossible at $R \simeq 108.429$ kΩ. Increasing the resistivity in a continuous loop would also decrease L_{crit} and $L_{\min}$. However, the speed of propagation being proportional to $1/\sqrt{\rho}$ in a continuous media [30], $\sqrt{\rho}L_{crit}(\rho)$ and $\sqrt{\rho}L_{\min}(\rho)$ would remain invariant. To compare the continuous and discrete medium, we computed the equivalent resistivity of the latter as

$$\rho_{equ}(R) = \rho + \frac{NR\pi a^2}{L} = \rho + \frac{R\pi a^2}{L_c}. \tag{5}$$

With this notation, R=0 corresponds to a continuous loop with resistivity ρ. If the two media were equivalent, the ratio

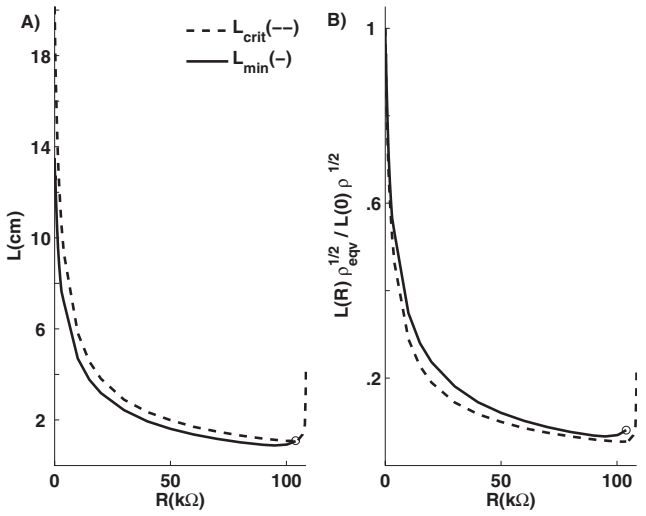

FIG. 1. (a) L_{crit} (cm, dashed line), the shortest L with period-1 reentry, and $L_{\min}$ (cm, solid line), the minimum L with QP reentry, as a function of the gap resistance R (kΩ). (b) Normalized values of L_{crit} and $L_{\min}=L_{crit,\min}(R)\sqrt{\rho_{eqv}(R)}/L_{crit,\min}(R=0)\sqrt{\rho}$ (see text).

$L(R)\sqrt{\rho_{eqv}(R)}/L(R=0)\sqrt{\rho}$ would remain equal to 1. Figure 1(b) shows clearly that the diminution of L_{crit} and $L_{\min}$ cannot be explained by a simple scaling, as it occurs in a continuous medium.

IV. L_{crit} AND P_{crit} IN TRANSITION TO QP REENTRY

Two distinct scenarios can lead to the disappearance of $P1$ reentry. For 108.429 kΩ$>R>$104 kΩ, sustained reentry does not exist for $L<L_{crit}=L_{\min}$, so that reentry ends abruptly with the disappearance of the $P1$ solution. For $R<104$ kΩ, $P1$ reentry is replaced by QP reentry, which persists from L_{crit} to $L_{\min}$. In this section, we consider the second type of transition. In the continuous MBR loop, the bifurcation from $P1$ to QP propagation occurs at the critical period $P_{crit}=D_{crit}+A_{crit}$ where D_{crit} and A_{crit} are the values for which the slope of the restitution curve $A(D)$ reaches 1 [6,9]. P_{crit} is constant and independent of ρ in a continuous medium. In contrast, Fig. 2(a) shows that P_{crit} increases with R in the discrete loop. Both A_{crit} and D_{crit} contribute to the change of P_{crit} [Fig. 2(b)], but the increase of D_{crit} is more important. For each value of R, we collected the D and A values of the $P1$ solutions for a set of L values close to L_{crit} as well as those of the first QP solution below L_{crit} to construct the $A(D)$ restitution curve. Each curve was fitted with a simple exponential to find $D_{crit,th}(R)$, the value where the slope of the fitted $A(D)=1$, and the theoretical value $P_{crit,th}=D_{crit,th}+A(D_{crit,th})$. As shown in Fig. 2(a), $P_{crit,th}$ falls very close to the P_{crit} values found by simulation. Hence, the mechanism responsible for the transition from $P1$ to QP reentry is the same in the continuous and discrete loops, and the increase of P_{crit} results from R transforming the restitution curve. The mechanisms responsible for the change of D and A can be identified in Fig. 3, which shows the action potentials of the first node in the three successive cells for increasing values of R. (top to bottom, $R=0$, 80, and 103 kΩ). Increasing R prolongs the latency of the action potential, defined as the time interval between the minimum diastolic potential and the beginning of the action potential, set at the maximum derivative in the upstroke (left column panels). Since latency is included in the diastolic interval, its increase translates as an increase of D.

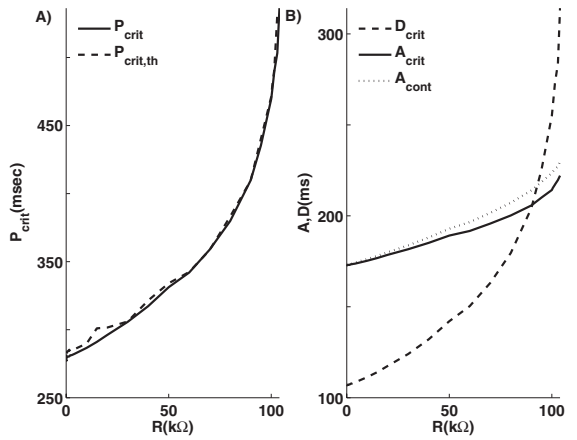

FIG. 2. (a) Solid line: for each value of the gap resistance R, the critical cycle length P_{crit} (ms) at L_{crit}, the shortest loop with period-1 reentry. Dashed line: $P_{crit,th}$, the critical cycle length computed from the restitution curve (see text). (b) Value of diastolic interval (D_{crit}, dashed line) and of the action potential duration (A_{crit}, solid line) at L_{crit}. The dotted line (A_{cont}) is the action potential duration for $P1$ solutions with $D=D_{crit}(R)$ on the continuous cable.

The mechanisms responsible for the change of A_{crit} and of the form of the restitution curve are complex and involve an interaction between the diffusive current and the gate variables, as it has been demonstrated in previous works [25,27]. Neighboring cells exchange current during the early phase of repolarization, which compensates for the delay of activation and tends to prolong the action potential. If the time course

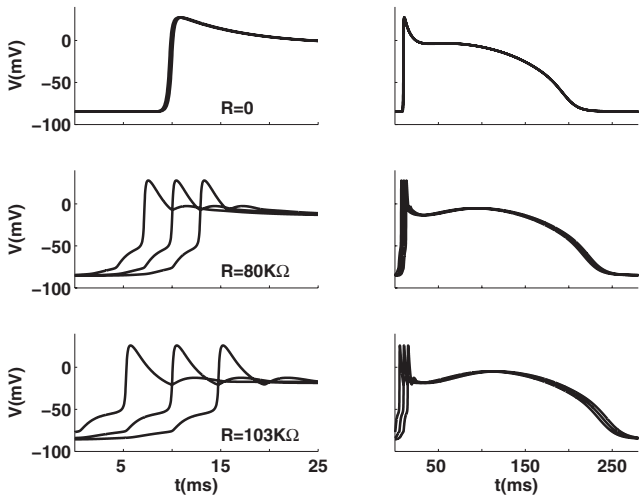

FIG. 3. Action potentials (mV) in the first node of three successive cells as a function of time (ms) during period-1 reentry for, from top to bottom, $R=0$, 80, and 103 kΩ. In the left-column panels, only the activation is shown, while the complete action potentials are displayed in the right-column panels.

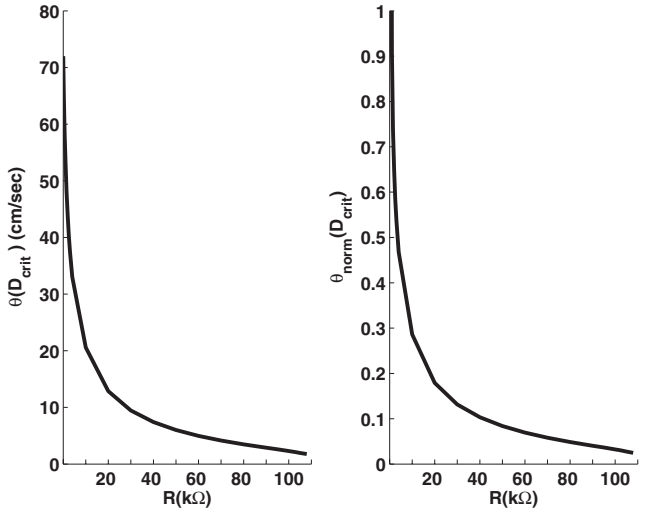

FIG. 4. Left panel: $\theta(D_{crit})$, the intercellular activation speed (calculated between the first node of successive cells, cm/s), at D_{crit} as a function of the gap resistance R. Right panel: $\theta_{norm}(D_{crit})$, normalized activation speed, defined as $\theta(D_{crit}(R))\sqrt{\rho_{eqv}(R)}/\theta_0(D_{crit}(R))\sqrt{\rho}$, where $\theta_0(D)$ is the speed of a period-1 solution with diastolic interval D in the continuous loop.

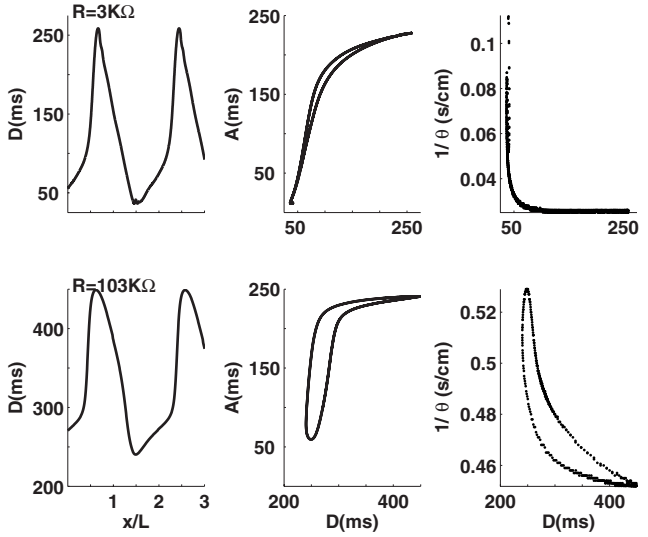

FIG. 5. Characteristics of the mode-0 QP solution at $L_{\min}$ for $R=3$ kΩ (top-row panels) and $R=103$ kΩ (bottom-row panels). Left panels: D, the diastolic interval, as a function of position (x/L) for three successive turns abutted end to end. Middle panels: A, the duration of the action potential, as a function of D, from the solutions shown in the left panels. Right panels: $1/\theta$, the cell-to-cell conduction time, as a function of D from the solutions shown in the left panels. Only the data of the first node of each cell were used to construct these plots.

of the gate variables of the calcium and potassium currents controlling the action potential duration was not concurrently altered during the subthreshold and early repolarization phase, $A_{crit}(R)$ would always be longer than $A_{cont}(D_{crit}(R))$, the duration of the action potential produced by an activation with $D=D_{crit}(R)$ on a continuous loop. As illustrated in Fig. 2(b), $A_{crit}(R)$ is always smaller that $A_{cont}(D_{crit}(R))$, which shows that the net effect of the diffusion current goes beyond a simple passive prolongation of the action potential.

Once P_{crit} is known, L_{crit} can be calculated if the speed of propagation, $\theta(D_{crit})$, is provided. In discrete media, the total time to propagate from one cell to another is a composite of the propagation time within and between the cells. The former decreases with R, while the latter, which is equivalent to the latency displayed in Fig. 3, increases. The final composite $\theta(D_{crit}(R))$ is shown in left panel of Fig. 4. In a continuous medium, $\theta_o(D)\sqrt{\rho}=c(D)$, where $c(D)$ is constant characterizing each value of D and $\theta_o(D)$ refers to the speed of a period-1 solution with diastolic interval D. Hence, $\theta_{norm}(D_{crit}(R))=\theta(D_{crit}(R))\sqrt{\rho_{eqv}(R)}/\theta_0(D_{crit}(R))\sqrt{\rho}$ would remain equal to 1 if R was acting on the speed only as a scaling factor, which is not the case as shown in the right panel of Fig. 4.

V. QP REENTRY

The characteristics of the QP reentry in the continuous MBR loop have been extensively discussed in previous papers [5–7]. Two modes of QP were identified, characterized by D and A oscillations with different spatial wavelengths (λ). The first mode, referred to as mode 0, exists from L_{crit} to $L_{\min}$. Its λ, close to two turns of the loop at L_{crit}, diminishes as the loop is shortened, but always remains longer than L. It appears through a supercritical bifurcation, in which the amplitude of D and A oscillation grows from zero as L is decreased below L_{crit}. The second, referred as mode 1, exists only over a subset of the $[L_{\min},L_{crit}]$ interval with λ always less than L. The mode-1 solution is created by a subcritical bifurcation at $L<L_{crit}$. These two types of QP solutions were found for all values of $R<104$ kΩ where QP solutions exist.

A. Mode-0 QP reentry

We first consider the mode-0 solutions that exist over the whole $[L_{\min},L_{crit}]$ interval. Figure 5 presents the characteristics of the mode-0 solutions at $L_{\min}$ for two values of R (top panels, $R=3$ kΩ, $L=7.65$ cm, bottom $R=103$ kΩ, $L=1.04$ cm). The leftmost panels show the spatial oscillation of D by plotting successive turns end to end. Similar mode-0 solutions were obtained for all $L\in[L_{\min}(R),L_{crit}(R)]$, characterized by stable D spatial profiles repeating with a wavelength $\lambda>L$. These solutions can be either periodic or quasiperiodic, depending whether λ is a rational or irrational fraction of L. Since λ decreases gradually as L is reduced, we chose to refer to them collectively as mode-0 quasiperiodic solutions.

Mode 0 solutions were also found to appear through a supercritical bifurcation with, as shown in Fig. 6, a gradual increases of the amplitude below L_{crit}. For these two cases, the nature of the bifurcation was further ascertained by prolonging the calculation up to 100 turns for L values close to L_{crit} and by enlarging the loop starting from $L<L_{crit}$ in the mode-0 QP regime.

An obvious difference between the left-column panels of Fig. 5 and between those of Fig. 6 is the range of D values

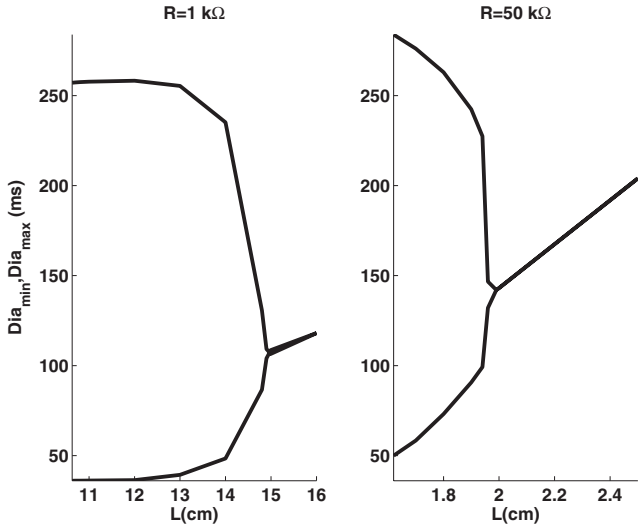

FIG. 6. D of the period-1 solution and from $L=L_{crit}$ $D_{\max}$ and $D_{\min}$ of the mode-0 QP solution as a function of L for $R=1$ kΩ (left panel) and 50 kΩ (right panel)

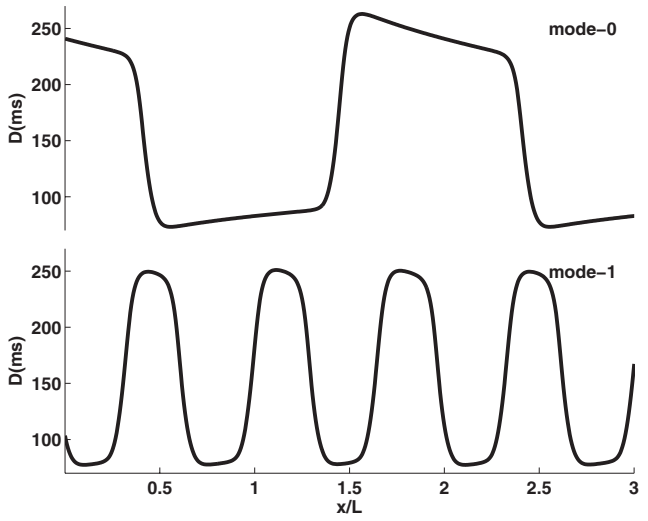

FIG. 8. Mode-0 (top panel) and mode-1 (bottom panel) QP solutions for $L=1.80$ cm and $R=50$ kΩ. The plots show D, the diastolic interval, as a function of position (x/L), for three turns abutted end to end.

covered by the solutions for different R. The left panel of Fig. 7 shows $D_{\min}$ and $D_{\max}$, the minimum and maximum values of D for the mode-0 solutions at $L_{\min}(R)$. It is well known that, in a discrete medium, the minimum excitability needed to sustain propagation increases as a function of R until a limiting value beyond which propagation is blocked even in a medium at rest [22]. In the MBR model, the excitability can be measured by the product hj of the inactivation gates of the sodium current. The right panel of Fig. 7 shows $hj(D_{\min})$ and $hj(D_{\max})$, the excitability of the action potentials produced, respectively, at $D_{\min}$ and $D_{\max}$ for the mode-0 solutions at $L_{\min}$. As R increases, the minimal excitability allowing propagation becomes higher, which requires an increase of $D_{\min}(R)$. At $R=104$ kΩ, $hj(D_{\min})=hj(D_{crit})$, QP

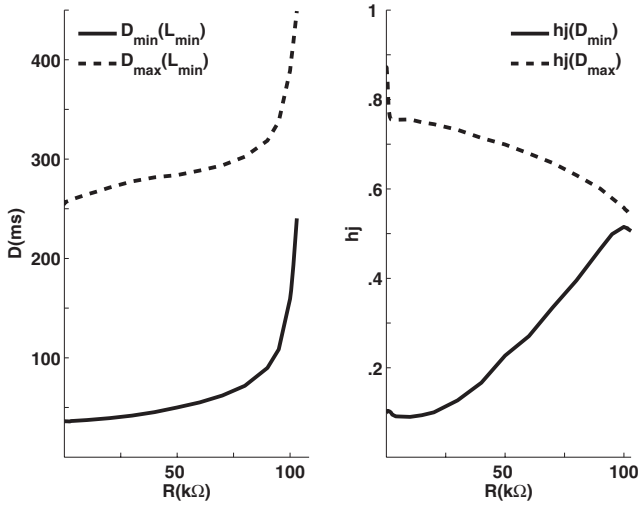

FIG. 7. Left panel: $D_{\min}$ (solid line) and $D_{\max}$ (dashed line)—respectively, the minimum and maximum diastolic intervals of the mode-0 QP solutions at $L_{\min}$ as a function of R. Right panel: hj, the product of the sodium current inactivation gates taken at $D_{\min}$ (solid line) and $D_{\max}$ (dashed line) for the mode-0 QP solutions at $L_{\min}$.

propagation disappears and only $P1$ reentry remains. On the other hand, the curve $hj(D_{\max})$ rather reflects the inactivation of the sodium current occurring during the latency preceding the upstroke of the longer action potential. At $R=104$ kΩ, the limit for QP propagation, $hj(D_{\max})>hj(D_{\min})=hj(D_{crit})$, which indicates that $P1$ propagation is still possible if R is increased. However, the difference is small, such that the range of R values over which $P1$ reentry can still occur is limited, as is seen in Fig. 1.

The middle column panels of in Fig. 5 display the $A(D)$ relation obtained from each QP mode-0 solution. Each curve has two branches, the lower and upper branches coming, respectively, from the increasing and decreasing portions of the D spatial profile. Such a dual structure has been observed in the continuous loop and was explained either by the influence of neighbors on the repolarization [18] or by short-term memory [15]. The separation between the branches is enhanced by the increase of R. Finally, the right column panels of Fig. 5 show $1/\theta$ vs D, the dispersion relation of the conduction time. For $R=3$ kΩ (top right panel), the dispersion relation appears as a single-value function, similar to what is seen in the MBR continuous loop. For $R=103$ kΩ (bottom right panel), the dispersion relation has two branches, as the $A(D)$ curve. The lower branch is associated with the decreasing portion of the D spatial profile.

B. Higher QP modes

Figure 8 shows an example of mode-0 and mode-1 solutions for $R=50$ kΩ and $L=1.8$ cm, in the middle of the $[L_{\min},L_{crit}]=[1.61$ cm, 1.99 cm$]$ interval for this value of R. Mode-1 solutions were found for all values of R with QP propagation over a subset of the $[L_{\min},L_{crit}]$ interval, as in the case of the continuous cable. Courtemanche *et al.* [10] in their analysis of a delay-integral model representing reentry on a 1D loop have predicted the existence of an infinite num-

ber of QP modes, with spatial wavelengths near L_{crit} given by

$$\lambda(n) = \frac{2L}{2n+1} - \frac{C}{(2n+1)^3}, \tag{6}$$

where n is the order of the mode and C is a small positive constant. As seen Fig. 8, $\lambda(0)/\lambda(1)$ is indeed close to 3. However, in the MBR continuous loop, only the first two modes (i.e., 0 and 1) were observed. This was explained by the effect of resistive coupling between neighbors that limits the spatial gradient of voltage and forbids the appearance of higher modes [7]. Theoretically,

$$\frac{\lambda(2)}{\lambda(0)} \simeq \frac{1}{5}, \quad \frac{\lambda(2)}{\lambda(1)} \simeq \frac{3}{5}. \tag{7}$$

To look for mode-2 solutions for different R and L values, we have compressed the D profiles of the mode-0 and mode-1 solutions up to, respectively, a factor of 6 and 2 to build different initial conditions. This procedure was successful in obtaining mode-1 solutions from mode-0 solutions, but higher modes of propagation were never produced. For all scaling factors, propagation was found to stabilize either to mode 0 or mode 1. It is noteworthy that mode-1 solutions always appeared at $L<L_{crit}$ with high-amplitude complex oscillations that damped as L was reduced, until reaching smooth patterns as the one shown in Fig. 8.

VI. DISCUSSION AND SUMMARY

Increasing R in the discrete loop allows sustained reentry to be maintained in much shorter circuits than in continuous loops with equivalent lumped resistance. The critical period at which the bifurcation from period-1 to QP propagation occurs can still be predicted from the $A(D)$ dispersion curve constructed by gathering data from $P1$ solutions and from mode-0 QP solutions close to supercritical bifurcation. However, increasing R modifies $A(D)$ and the value of P_{crit}. On the one hand, the latency of the cell-to-cell propagation is augmented due to the decrease of the intercellular current. This prolongs D, which includes the latency and pushes $A(D)$ to the right. The partial closure of the sodium current inactivation gates, which occurs during slow depolarization, increases the voltage threshold and also contributes to the prolongation of D. In space-clamped models, changing the amplitude [25] or the duration of square pulse stimuli [31] modifies the $A(D)$ restitution curve. Hence, the change of the subthreshold depolarization coming with higher R impacts on the restitution curve, together with the diffusion current in the early repolarization phase that influences the time course of the membrane voltage and of the gate variables. The increase of P_{crit} and the change of $A(D)$ are in line with the results of Qu [25] who found, using a Luo-Rudy-1 paced cable with nodes linked by discrete resistances, that reducing the coupling displaced the onset of alternans toward higher stimulation periods.

The shift of P_{crit} depends on both the change of D_{crit} and $A(D_{crit})$. In order to analyze these effects, it would be more appropriate to separate the latency from the diastolic interval, redefining D from the end of the action potential to the minimum of V in repolarization and considering the latency *lat* to extend from the end of D to the maximum derivative of the upstroke [32]. Then both A and *lat* could be analyzed as functions of D and R. However, even with this change, it will be difficult to build a low-dimensional equivalent model of the propagation, extending the integral-delay model developed for the continuous loop. As seen in Fig. 5, increasing R enhances the dual structure of $A(D)$ during propagation. Moreover, a similar type of dual structure also appears for $1/\theta$, which is almost equivalent to the latency at high R values. It thus becomes impossible to neglect the modulating effect of coupling on both A and θ at high R values. Whether alternative approaches that have been proposed for the continuous loop would be more appropriate remains to be determined [11,16,17]. In any case, we are still far from a general low-dimensional model that could also be applied in situations including a dynamic change of the intercellular coupling, as in [33–35].

R also influences $L_{\min}$, the minimal length with QP propagation. Because higher R necessitates more excitability for propagation, the minimum D in sustained QP reentry increases until it reaches $D_{crit}(R)$. From this value of R, QP propagation becomes impossible. For R above this limiting value, period-1 reentry ends abruptly when its D reaches the minimal value allowing propagation. The minimal L for propagation increases until R reaches the value where propagation becomes impossible even in a medium at rest. Again, it would be very interesting to study reentry in a medium with dynamical modulation of the gap resistance.

In all cases with QP propagation, we found the bifurcation from period-1 to mode-0 propagation to be supercritical. For some R values, the nature of the bifurcation was further ascertained by prolonging the simulation up to 100 rotations and by expanding the loop from a length with QP propagation. It cannot be excluded that the bifurcation was misclassified at least for some values of R because of prolonged slow growing transients. A numerical analysis of an integral-delay model of reentry has shown that increasing the slope of the $A(D)$ function could turn the bifurcation from super to subcritical [7]. Since Qu [25] has reported that reduced coupling increases the slope of $A(D)$ at least at short D values and since Fig. 5 also shows that it increases the steepness of the restitution relation, the increase of R was expected to change the bifurcation. However, the nature of the bifurcation, which is determined by the response of the system to small perturbations around the period-1 solution, is controlled by the variation of the slope close to D_{crit}. In our case where the $A(D)$ functions were constructed from stable solutions close to $L_{crit}(R)$, we observed a minimal increase of the steepness of the function around D_{crit} for all values of R. This may explain why the bifurcation has remained supercritical, and it does not exclude the possibility that it could be different for other ionic models.

As in the continuous case, mode-1 solutions were found to exist in a subset on the $[L_{\min}, L_{crit}]$ interval. We also devoted much effort to finding $n>1$ modes of QP propagation for different values of R, building initial conditions either from mode-0 or mode-1 solutions for different L within the $[L_{\min}, L_{crit}]$ interval. All these attempts were unsuccessful. Our initial guess was that the increase of R should allow more abrupt gradients of potential to exist between the cells, thus permitting the existence of higher modes of propagation. However, as seen in Fig. 5, the dual structure of the $A(D)$ and $1/\theta$ relations becomes more pronounced at high R. This suggests that coupling still limits the gradient below what would be needed for higher modes of propagation.

This work was supported by a grant from the Natural Sciences and Engineering Research Council of Canada.

[1] L. Boersma, J. Brugada, C. J. H. Kirchhof, and M. A. Allessie, Circulation **88**, 1852 (1993).
[2] J. Brugada, L. Boersma, C. J. H. Kirchhof, V. V. Heynen, and M. A. Allessie, Circulation **84**, 1296 (1991).
[3] L. H. Frame and M. B. Simson, Circulation **78**, 1277 (1988).
[4] P. L. Rensma, M. A. Allessie, W. J. E. P. Lammers, F. I. M. Bonke, and M. J. Schalij, Circ. Res. **62**, 395 (1988).
[5] A. Vinet and L. J. Leon, *Proc. 13th IEEE/EMDSSS* (1991), p. 508.
[6] A. Vinet and F. A. Roberge, Ann. Biomed. Eng. **22**, 568 (1994).
[7] A. Vinet, Ann. Biomed. Eng. **28**, 704 (2000).
[8] A. Vinet, J. Biol. Syst. **7**, 451 (1999).
[9] M. Courtemanche, L. Glass, and J. P. Keener, Phys. Rev. Lett. **70**, 2182 (1993).
[10] M. Courtemanche, J. P. Keener, and L. Glass, J. Appl. Math. **56**, 119 (1996).
[11] B. Echebarria and A. Karma, Phys. Rev. Lett. **88**, 208101 (2002).
[12] A. Karma, Phys. Rev. Lett. **71**, 1103 (1993).
[13] T. J. Lewis and M. R. Guevara, J. Theor. Biol. **146**, 407 (1990).
[14] W. Quan and Y. Rudy, Circ. Res. **66**, 367 (1990).
[15] X. Chen, F. H. Fenton, and R. A. Gray, Heart Rhythm **2**, 1038 (2005).
[16] E. Cytrynbaum and J. P. Keener, Chaos **12**, 788 (2002).
[17] G. A. Gottwald and L. Kramer, Chaos **16**, 013122 (2006).
[18] P. Comtois and A. Vinet, Phys. Rev. E **68**, 051903 (2003).
[19] M. S. Spach and J. F. Heidlage, Circ. Res. **76**, 366 (1995).
[20] J. P. Keener, J. Theor. Biol. **148**, 49 (1991).
[21] Y. Rudy, J. Cardiovasc. Electrophysiol. **6**, 294 (1995).
[22] V. G. Fast and A. G. Kléber, Circ. Res. **73**, 914 (1993).
[23] Y. Rudy and W. L. Quan, Circ. Res. **61**, 815 (1987).
[24] R. M. Shaw and Y. Rudy, Circ. Res. **81**, 727 (1997).
[25] Z. Qu, Am. J. Physiol. **287**, H2803 (2004).
[26] Z. Qu, H. R. Karagueuzian, A. Garfinkel, and J. N. Weiss, Am. J. Physiol. **286**, H2803 (2004).
[27] E. M. Cherry and F. H. Fenton, Am. J. Physiol. **286**, H2332 (2004).
[28] F. A. Roberge, A. Vinet, and B. Victorri, Circ. Res. **58**, 461 (1986).
[29] P. Comtois and A. Vinet, Phys. Rev. E **72**, 051927 (2005).
[30] A. G. Kléber, C. B. Riegger, and M. J. Janse, Circ. Res. **61**, 271 (1987).
[31] A. Vinet, D. R. Chialvo, and J. Jalife, Ann. (N.Y.) Acad. Sci. **601**, 281 (1990).
[32] A. Vinet, D. R. Chialvo, D. C. Michaels, and J. Jalife, Circ. Res. **67**, 1510 (1990).
[33] R. Jamaleddine and A. Vinet, J. Biol. Syst. **7**, 475 (1999).
[34] A. P. Henriquez, R. Vogel, B. J. Muller-Borer, C. S. Henriquez, R. Weingart, and W. E. Casio, Biophys. J. **81**, 2112 (2001).
[35] C. Oka, H. Matsuda, N. Sarai, and A. Noma, J. Physiol. Sci. **56**, 79 (2006).